

# Creation of entangled atomic states by an analogue of the Dynamical Casimir Effect

K. Lange<sup>1</sup>, J. Peise<sup>1</sup>, B. Lücke<sup>1</sup>, T. Gruber<sup>2</sup>, A. Sala<sup>3</sup>, A. Polls<sup>4,5</sup>, W. Ertmer<sup>1</sup>, B. Juliá-Díaz<sup>4,5</sup>, L. Santos<sup>2</sup>, C. Klempt<sup>1</sup>

<sup>1</sup>Institut für Quantenoptik, Leibniz Universität Hannover, Welfengarten 1, D-30167 Hannover, Germany

<sup>2</sup>Institut für Theoretische Physik, Leibniz Universität Hannover, Appelstraße 2, D-30167 Hannover, Germany

<sup>3</sup>Department of Physics, NTNU, Norwegian University of Science and Technology, 7491 Trondheim, Norway

<sup>4</sup>Departament de Física Quàntica i Astrofísica, Facultat de Física, Universitat de Barcelona, Barcelona 08028, Spain

<sup>5</sup>Institut de Ciències del Cosmos, Universitat de Barcelona, ICCUB, Mart i Franquès 1, Barcelona 08028, Spain

E-mail: lange@iqo.uni-hannover.de

**Abstract.** If the boundary conditions of the quantum vacuum are changed in time, quantum field theory predicts that real, observable particles can be created in the initially empty modes. Here, we realize this effect by changing the boundary conditions of a spinor Bose-Einstein condensate, which yields a population of initially unoccupied spatial and spin excitations. We prove that the excitations are created as entangled excitation pairs by certifying continuous-variable entanglement within the many-particle output state.

## 1. Introduction

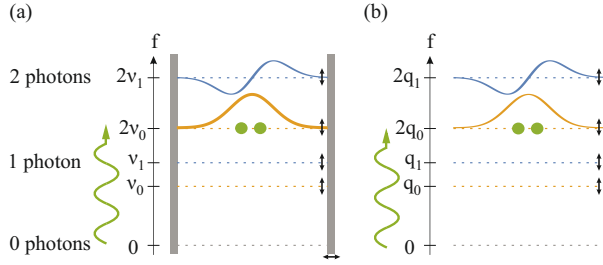


**Figure 1.** (a) Schematic principle of the originally proposed Dynamical Casimir effect. The system includes two perfectly conducting plates which allow for a discrete spectrum of modes which may be populated with photons. Changing the distance of plates non-adiabatically will result in an energetic shift of the light modes (black arrows). If the frequency of the modulation (green arrow) is resonant to a certain mode, a pair of virtual photons is turned into real photons (green circles). (b) Our analogue setup: By manipulating the energy difference of the Zeeman levels, we can excite spins out of our spinor Bose-Einstein condensate blue into initially empty modes.

The quantized vacuum contains pairs of virtual quanta in all available modes of the physical system. The static Casimir effect [1] is a measurable consequence of this process. In the original setting, two mirrors experience an attractive interaction due to the reduced number of electromagnetic modes in the volume between them. First attempted in 1956 [2], the Casimir force was precisely measured in the late 1990s [3, 4]. If the mode density is not varied in space but in time, for example by a modulation of the mirror's distance, the virtual quanta can be turned into macroscopic numbers of real excitations (see Fig. 1a). The excitations are created pairwise - leading to the generation of entangled many-particle states out of the vacuum. This so-called Dynamical Casimir effect (DCE) [5, 6] has been observed in the microwave regime [7, 8]. Bose-Einstein condensates (BECs) of diluted gases offer the possibility to study this effect by driving spatial excitations [9] or spin excitations [10] through the modulation of the system's boundary conditions. While Ref. [10] demonstrates the suppression of thermal excitations and a squeezing of spin-nematic observables, a proof that the DCE creates entanglement is missing.

In this article, we demonstrate the excitation of both spin and spatial degrees of freedom in a spinor BEC by the DCE. We prove that the spin excitations are

created in the form of entangled pairs by a violation of a continuous-variable entanglement criterion [11, 12]. The experimental data is supported by a theoretical description of the system in terms of a numerical Bogoliubov analysis.

## 2. Theoretical description

We consider an  $F = 1$  spinor BEC initially prepared in  $m = 0$ . The system is described by the bosonic operators  $\hat{\psi}_m(\vec{r})$  that annihilate atoms with spin  $m$  at position  $\vec{r}$ . Using Bogoliubov's approximation  $\hat{\psi}_0(\vec{r}) = \psi_0(\vec{r}) + \delta\psi_0(\vec{r})$ , where  $\psi_0(\vec{r})$  is the mean-field, and  $\delta\psi_0(\vec{r})$  denote scalar fluctuations of the  $m = 0$  condensate. Up to second-order in the fluctuations, the spin fluctuations  $\psi_{\pm 1}(\vec{r})$  decouple from the scalar fluctuations, and are given by the Hamiltonian:

$$\hat{H}_1 = \sum_{m=\pm 1} \int d^3r \hat{\psi}_m^\dagger(\vec{r}) \left( \hat{H}_{\text{eff}} + q \right) \psi_m(\vec{r}) + U_1 \int d^3r n_0(\vec{r}) \left( \hat{\psi}_1^\dagger(\vec{r}) \hat{\psi}_{-1}^\dagger(\vec{r}) + \text{H.c.} \right) \quad (1)$$

where  $\hat{H}_{\text{eff}} = -\hbar^2 \nabla^2 / 2M + V(\vec{r}) + (U_0 + U_1)n_0(\vec{r}) - \mu$ , with  $M$  the atomic mass,  $n_0(\vec{r}) = |\psi_0(\vec{r})|^2$ ,  $V(\vec{r})$  the external trapping,  $\mu$  the chemical potential,  $U_0 = (g_0 + 2g_2)/3$ ,  $U_1 = (g_2 - g_0)/3$ , and  $g_F = 4\pi\hbar^2 a_F / M$ , with  $a_F$  the scattering-length for the collisional channel with total spin  $F$ . In Eq. (2),  $q$  denotes the quadratic Zeeman energy (QZE) term. This energy may be externally modified using microwave fields. In particular  $q$  may be modified in time, which is a key feature in the following (see Fig. 1b).

### 2.1. Free space

The connection between the spin dynamics in the presence of a time-dependent QZE and the DCE becomes particularly evident when considering a homogeneous BEC, i.e.  $V(\vec{r}) = 0$ . In that case,  $n_0(\vec{r}) = n$  is a constant, and Eq. (2) may be re-written in momentum,  $k$ , space:

$$\hat{H}_1 = \sum_k \left[ \sum_{m=\pm 1} \left( \frac{\hbar^2 k^2}{2M} + nU_1 + q \right) \hat{a}_{k,m}^\dagger \hat{a}_{k,m} + U_1 \left( \hat{a}_{k,1}^\dagger \hat{a}_{k,-1}^\dagger + \text{H.c.} \right) \right]. \quad (2)$$

Employing the operators  $\hat{a}_\pm = (\hat{a}_1 \pm \hat{a}_{-1})/\sqrt{2}$ , we introduce the Bogoliubov transformation  $\hat{a}_{k,\pm} =$

$\cosh \alpha_{k,\pm} \hat{b}_{k,\pm} + \sinh \alpha_{k,\pm} \hat{b}_{-k,\pm}^\dagger$ , with  $\tanh \alpha_{k,\pm} = -nU_1/\xi(k)$ , where

$\xi(k) = \sqrt{(\hbar^2 k^2/2M + q)(\hbar^2 k^2/2M + q + 2U_1 n)}$  is the Bogoliubov spectrum of spin excitations. Using this transformation

$$\hat{H}_1 = \sum_k \xi(k) \left( \hat{b}_{k,+}^\dagger \hat{b}_{k,+} + \hat{b}_{k,-}^\dagger \hat{b}_{k,-} \right).$$

For the case of sudden quench of the QZE from an initial value  $q_i$  to a final one  $q_f$ , we introduce the Bogoliubov modes  $\hat{a}_{k,\pm} = \cosh \alpha_{k,\pm} \hat{b}_{k,\pm} + \sinh \alpha_{k,\pm} \hat{b}_{-k,\pm}^\dagger$ , evaluated for  $q_i$ , and  $\hat{a}_{k,\pm} = \cosh \tilde{\alpha}_{k,\pm} \hat{c}_{k,\pm} + \sinh \tilde{\alpha}_{k,\pm} \hat{c}_{-k,\pm}^\dagger$ , evaluated for  $q_f$ . The initial Bogoliubov modes fulfill the vacuum statistics  $\langle \hat{b}_{k,\pm}^\dagger \hat{b}_{k,\pm} \rangle = 0$ . When quenching  $q$ , the initial Bogoliubov modes project into the new ones:  $c_{k,\pm} = \cosh \Delta \alpha_{k,\pm} b_{k,\pm} - \sinh \Delta \alpha_{k,\pm} b_{-k,\pm}^\dagger$ , with  $\Delta \alpha_{k,\pm} = \tilde{\alpha}_{k,\pm} - \alpha_{k,\pm}$ . As a result, as for the traditional Casimir effect, the quench of the QZE results in non-zero occupations of the new Bogoliubov modes,  $\langle \hat{c}_{k,\pm}^\dagger \hat{c}_{k,\pm} \rangle = \sinh^2 \Delta \alpha_{k,\pm}$ . In addition,  $\langle \hat{c}_{k,\pm}^\dagger \hat{c}_{-k,\pm} \rangle = -\frac{1}{2} \sinh 2\Delta \alpha_{k,\pm}$ . After the quench, the evolution of the Bogoliubov modes is trivial  $\hat{c}_{k,\pm}(t) = e^{-i\xi_f(k)t/\hbar} \hat{c}_{k,\pm}(0)$ , where  $\xi_f(k)$  is calculated for  $q_f$ .

This occupation of the spin Bogoliubov modes results in the creation of particles in  $|F, m\rangle = |1, \pm 1\rangle$ . Indeed, using the relation between  $\hat{a}_{k,\pm}$  and  $\hat{c}_{k,\pm}$ , we may obtain the population in  $|1, 1\rangle$ ,  $n_{k,1}(t) = \langle \hat{a}_{k,1}^\dagger \hat{a}_{k,1} \rangle$ , which is at any time equal to that in  $|1, -1\rangle$ :

$$\begin{aligned} n_{k,1}(t) &= \cosh^2 \tilde{\alpha}_{k,\pm} \sinh^2 \Delta \alpha_{k,\pm} \\ &+ \sinh^2 \tilde{\alpha}_{k,\pm} \cosh^2 \Delta \alpha_{k,\pm} \\ &- \frac{1}{2} \cos(2\xi(k)t/\hbar) \sinh 2\tilde{\alpha}_{k,\pm} \sinh 2\Delta \alpha_{k,\pm}. \end{aligned} \quad (3)$$

Assuming a large  $q_i \gg nU_1$ , we may approximate  $\alpha_{k,\pm} \simeq 0$ , and hence

$$n_{k,\pm 1}(t) = \left( 1 - \cos\left(\frac{2\xi_f(k)t}{\hbar}\right) \right) \left( \frac{U_1 n}{\xi_f(k)} \right)^2. \quad (4)$$

This creation of particles in the levels  $|1, \pm 1\rangle$  constitutes the spin analogue of the recently reported Sakharov oscillations observed in scalar BECs when quenching the interactions [13].

On the other hand, if  $q(t)$  is periodically modulated in time, the resulting spinor dynamics resembles the DCE. The Heisenberg equations for the Bogoliubov modes are of the form:

$$\frac{d}{dt} \hat{b}_{k,\pm} = -if_k \hat{b}_{k,\pm} \pm g_k \hat{b}_{-k,\pm}, \quad (5)$$

where  $f_k \equiv \xi(k)/\hbar$  and  $g_k = -\frac{dq}{dt} nU_1/2\xi(k)^2$ . We introduce the expected values  $P_k \equiv \langle \hat{b}_{k,\pm}^\dagger \hat{b}_{k,\pm} \rangle$ ,  $S_k \equiv \pm \langle \hat{b}_{k,\pm}^\dagger \hat{b}_{-k,\pm}^\dagger \rangle + \text{H.c.}$ , and  $A_k \equiv \pm i \left( \langle \hat{b}_{k,\pm}^\dagger \hat{b}_{-k,\pm}^\dagger \rangle - \text{H.c.} \right)$ . The dynamics of these expected values is given by the equations:

$$\dot{P}_k = g_k S_k, \quad (6)$$

$$\dot{S}_k = 4g_k P_k + 2g_k + 2f_k A_k, \quad (7)$$

$$\dot{A}_k = -2f_k S_k, \quad (8)$$

The population in  $m = \pm 1$  is given by:

$$\begin{aligned} n_{k,\pm 1}(t) &= \frac{\hbar^2 k^2/2M + q + nU_1}{\xi(k)} \left( P_k(t) + \frac{1}{2} \right) \\ &- \frac{1}{2} - \frac{U_1 n}{\xi(k)} S_k(t), \end{aligned} \quad (9)$$

which generalizes Eqs. (3) and (4). Hence, as for the quench, the time dependent QZE results in a DCE, where the number of particles may be significantly enhanced employing a periodically-modulated  $q(t)$  with a frequency matching resonantly a natural one.

## 2.2. Trapped case

The analysis of the experimental realization of the Casimir effect demands a careful consideration of the trapping potential. In order to determine  $\hat{H}_{\text{eff}}$ , we first obtain the initial density profile  $n_0(\vec{r})$  from the corresponding scalar Gross-Pitaevskii equation:

$$\mu \psi_0(\vec{r}) = \left[ -\frac{\hbar^2 \nabla^2}{2M} + V(\vec{r}) + U_0 n_0(\vec{r}) \right] \psi_0(\vec{r}). \quad (10)$$

We then evaluate the eigenfunctions  $\varphi_j(\vec{r})$  of  $\hat{H}_{\text{eff}}$ , such that  $\hat{H}_{\text{eff}} \varphi_j(\vec{r}) = E_j \varphi_j(\vec{r})$ . Expressing  $\hat{\psi}_m(\vec{r}) = \sum_j \varphi_j(\vec{r}) \hat{a}_{j,m}$ , we may re-express:

$$\begin{aligned} \hat{H}_1 &= \sum_{j,m=\pm 1} (E_j + q) \hat{a}_{j,m}^\dagger \hat{a}_{j,m} \\ &+ U_1 \sum_{i,j} \chi_{i,j} \left( \hat{a}_{i,1}^\dagger \hat{a}_{j,-1}^\dagger + \text{H.c.} \right), \end{aligned} \quad (11)$$

with  $\chi_{i,j} = \int d^3 r n_0(\vec{r}) \varphi_i(\vec{r}) \varphi_j(\vec{r})$ . For a sufficiently tight confinement, we may assume  $\chi_{i,j \neq i} \ll \chi_{i,i}$ , and  $U_1 \chi_{i,j \neq i} \ll |E_i - E_j|$  (this is indeed the case for our experimental parameters). In that case,  $\hat{H}_1 \simeq \sum_j \hat{h}_j$ , with  $\hat{h}_j = (E_j + q) \sum_{m=\pm 1} \hat{a}_{j,m}^\dagger \hat{a}_{j,m} + U_1 \chi_{jj} \left( \hat{a}_{j,1}^\dagger \hat{a}_{j,-1}^\dagger + \text{H.c.} \right)$ . We may then introduce the Bogoliubov transformation  $\hat{a}_{j,1} = \cosh \alpha_j \hat{b}_{j,+} + \sinh \alpha_j \hat{b}_{j,-}^\dagger$ , and  $\hat{a}_{j,-1} = \cosh \alpha_j \hat{b}_{j,-} + \sinh \alpha_j \hat{b}_{j,+}^\dagger$ , with  $\tanh 2\alpha_j = -U_1 \chi_{jj}/(E_j + q)$ . Then, apart from constants,  $\hat{h}_j = \xi_j \left( \hat{b}_{j,+}^\dagger \hat{b}_{j,+} + \hat{b}_{j,-}^\dagger \hat{b}_{j,-} \right)$ , where  $\xi_j = \sqrt{(E_j + q)^2 - (U_1 \chi_{jj})^2}$  are the corresponding Bogoliubov energies.

We may proceed at this point as for the free-space case, obtaining the equations for the dynamics of the Bogoliubov modes:  $\frac{d}{dt} \hat{b}_{j,\pm} = \mp i f_j b_{j,\pm} + g_j \hat{b}_{j,\mp}^\dagger$ , with  $f_j = \xi_j/\hbar$ , and  $g_j = \dot{q} U_1 \chi_{jj}/2\xi_j$ . We introduce  $P_j \equiv \langle \hat{b}_{j,\pm}^\dagger \hat{b}_{j,\pm} \rangle$ ,  $S_j \equiv \langle \hat{b}_{j,+}^\dagger \hat{b}_{j,-}^\dagger \rangle + \text{c.c.}$ , and  $A_j \equiv i \left( \langle \hat{b}_{j,+}^\dagger \hat{b}_{j,-}^\dagger \rangle - \text{c.c.} \right)$ . Thus, the results for the trapped case resemble the free-space results by replacing the momentum states by eigenstates of the effective potential.

### 3. Experimental observation

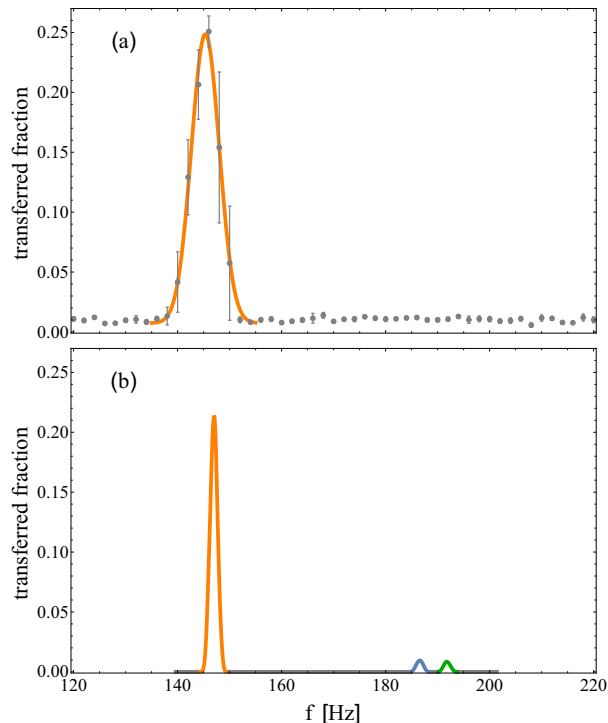


**Figure 2.** The relative number of atoms in the  $m = \pm 1$  levels is shown as function of the modulation frequency  $f$  of the quadratic Zeeman energy. (a) Experimental results with one clearly visible resonance corresponding to the ground mode. The full orange line is a Gaussian fit, yielding a resonance frequency of 145 Hz. The maximum transfer corresponds to an excitation creation rate of  $\Omega/2\pi = 1.06$  Hz. (b) The theoretical calculations show one clearly visible resonance at 147 Hz with a corresponding excitation creation rate of  $\Omega/2\pi = 1.01$  Hz. Both the position and the creation rates match the experimental results. Two smaller resonances are also visible at the frequencies 187 Hz and 192 Hz, corresponding to spatially excited modes.

We employ almost pure  $^{87}\text{Rb}$  BECs in a crossed-beam optical dipole trap with trapping frequencies  $2\pi \times (150, 160, 220)$  Hz. The 22,000 atoms in the BEC are prepared in the hyperfine level  $|1, 0\rangle$ . At our applied magnetic field of  $B = 2.6$  G, the magnetic field-induced QZE is  $q_B = 487$  Hz. Before initiating the dynamics, we empty the levels  $|1, \pm 1\rangle$  with two microwave pulses from  $|1, \pm 1\rangle$  to  $|2, \pm 2\rangle$  followed by a light push resonant to the  $F=2$  manifold to ensure that there are no excitations present in these levels. In our experiments, we apply an effective shift of the QZE  $q_d$  by a microwave dressing field that couples the levels  $|1, -1\rangle$  and  $|2, -2\rangle$ . When the dressing field compensates the magnetic-field-induced QZE almost completely,  $q = q_B + q_d = q_0$ , the transfer of atoms from  $|1, 0\rangle$  to  $|1, \pm 1\rangle$  in the trap's ground mode becomes energetically allowed. We thus observe a resonance condition, where the QZE allows for a maximal instability rate  $\xi_j$  according to the Hamiltonian in

eq. (11) [14, 15, 16] (see Fig. 3a). There are further resonances at  $q = q_j < q_0$ , when the difference  $q_0 - q_j$  is approximately equal to the energy difference  $E_j - E_0$  to the  $j$ th excited mode of the effective potential. In our experiments, the first two excited spatial modes are seen as one resonance, because two trap frequencies are close to degeneracy. Nevertheless, as shown with the absorption images, they can be individually addressed by choosing the correct QZE.

The analogue DCE is realized in the regime  $q > q_0$ , where the BEC is stable. Here, the intensity of the microwave field is modulated sinusoidally, yielding a corresponding oscillation of the QZE. If the frequency of the QZE oscillation is resonant to approximately twice the QZE difference to a specific resonance,  $f = 2(q - q_j)/h$ , atoms are parametrically excited to the respective mode. This process can be described as a parametric amplification of vacuum fluctuations in the  $|1, \pm 1\rangle$  modes. The number of the transferred atoms is detected by state-selective absorption imaging. We will show that the amplification of vacuum fluctuations leads to measurable populations in the levels  $|1, \pm 1\rangle$  in spin and spatial degrees of freedom and confirm the quantum origin of the dynamics by quantifying the created continuous-variable entanglement.

#### 3.1. Dynamical Casimir ground-mode resonance

In our experiments, we observe the analogue DCE by setting the QZE to a value of  $q - q_0 = h \times 71$  Hz, far in the stable regime. We modulate the QZE for 700 ms with an amplitude of  $h \times 48$  Hz by controlling the intensity of the microwave dressing field. Figure 2a shows the fraction of transferred atoms as a function of the modulation frequency  $f$ . The data shows a resonance at 145 Hz, which is approximately twice the QZE difference to the ground mode,  $2(q - q_0) = h \times 142$  Hz. The data may be compared to the theoretical prediction in Fig. 2b. Here, the frequency of the ground-mode resonance at 147 Hz is in good agreement with the experimental results. On resonance, the transferred fraction of atoms follows an exponential growth. We calculate a theoretical spin excitation rate of  $\Omega/2\pi = 1.01$  Hz that matches well the experimental rate of  $\Omega/2\pi = 1.06$  Hz, as it is obtained from the maximally transferred fraction on resonance. In contrast to the theoretical calculations, the experimental resonance width of 2.7 Hz is four times larger than the width of the theoretical resonance of 0.7 Hz. This is a result of the varying total number of atoms in our BECs as discussed below. The excited state resonances at the frequencies 187 Hz and 192 Hz are not visible in our experimental data. We will address this issue in the next paragraph.

## 3.2. Excited resonance

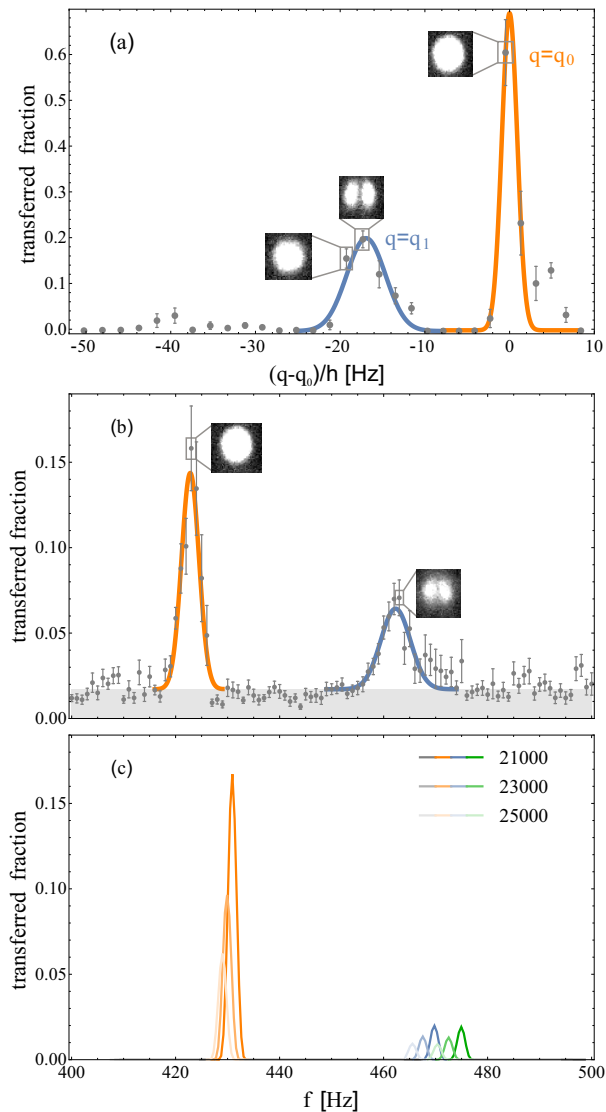


**Figure 3.** (a) For specific values of the QZE  $q = q_j$ , we observe well resolved resonances, where distinct spatial modes are populated via spin dynamics towards the levels  $|1, \pm 1\rangle$ . The spatial profile of the modes is observed in our absorption images (see inset). The colored lines are Gaussian fits to guide the eye. (b) Parametric excitations populate distinct resonances by varying the modulation frequency of the quadratic Zeeman energy after generating seed atoms with collisional interactions. The gray shaded area indicates the mean transfer due to spin-changing collisions. Same colors indicate the same modes. (c) Theoretically obtained resonances for different total numbers of atoms. The brightness corresponds to different total number of atoms and different colors indicate different modes.

We further study the analogue DCE on an excited spatial mode. As seen in Fig. 2b, the creation rate of excitations is smaller and narrower for excited spatial modes due to the reduced mode overlap  $\chi_{jj}$ . For such reduced spin excitation rates, our system is dominated by additional loss processes, such as atomic

collisions that transfer the atoms from the excited trap mode to the ground mode. As the exponential growth rate depends on the bosonic enhancement of initially transferred atoms, a significant loss can lead to a complete inhibition of the growth process. Furthermore, fluctuations of the total number of atoms lead to a further suppression of the resonance, as discussed below.

To mitigate the influence of the loss processes, we enhance the creation rate on the first excited spatial mode by an initial transfer of seed atoms to the chosen mode. Prior to our DCE protocol, we deliberately transfer seed atoms to the first excited spatial mode by choosing a resonant QZE  $q = q_1$  (see Fig. 3a). The creation of seed atoms is facilitated by enabling spin-changing collisions via our microwave dressing for 150 ms on the first excited spatial mode at  $q - q_0 = -h \times 16.9$  Hz. In the mean, 1.7% of the atoms are transferred to the excited spatial mode (gray shaded area in Fig. 3b).

We further increase the signal by increasing the modulation amplitude. We oscillate  $q$  from  $h \times 45$  Hz to  $h \times 363$  Hz for a modulation time of 650 ms. Due to a nonlinearity, the oscillation is slightly distorted from a pure sinusoidal shape and is centered around  $h \times 214$  Hz. For these experimental parameters, we observe not only the population of the ground mode of the effective potential, but also of the seeded first excited mode (see Fig. 3b). The frequencies of the ground-mode and the excited-mode resonances are determined by Gaussian fits yielding 422 Hz and 462 Hz. The inset in Fig. 3b shows the spatial mode profile of the excited atoms. Resonances corresponding to a certain mode display the respective spatial profile.

The theoretical calculations in Fig. 3c agree qualitatively with the experimental results. The results are displayed for three different total numbers of atoms. The positions of the excited-mode resonances shift several resonance widths depending on the number of atoms. This number-dependent shift of the narrow lines combined with our experimental fluctuations of the total atoms number of 1800 atoms presents a reason why we were unable to observe the excited resonances without seed atoms. Furthermore, the theoretical results show a systematic shift to higher modulation frequencies compared to the experimental results. This effect may be explained by slight inaccuracies in the determination of the modulated QZE from dc measurements, as well as drifts and anharmonicities in the trapping potential.

Our results show the parametric excitation of atoms into different spin and spatial modes by an analogue of the DCE.

#### 4. Entanglement characterization

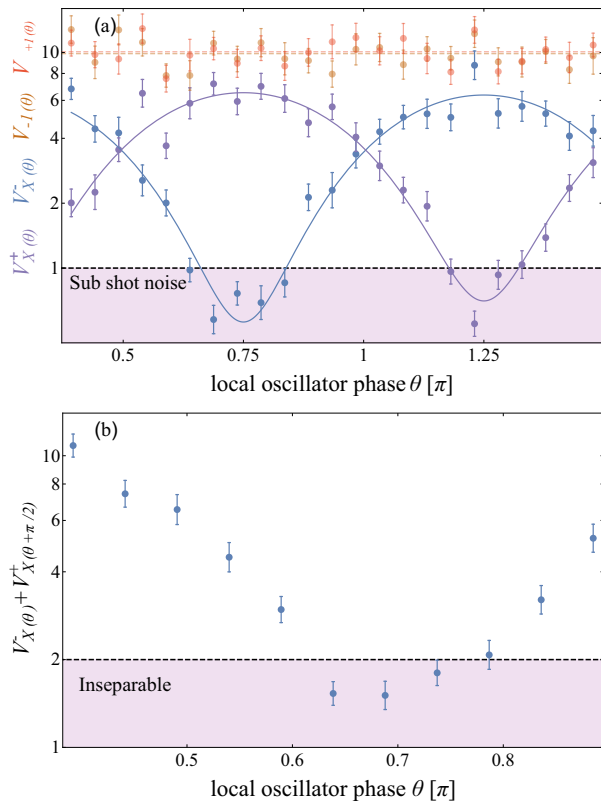


**Figure 4.** (a) One-mode variances  $V_{-1(\theta)}$  and  $V_{+1(\theta)}$  and two-mode variances  $V_{X(\theta)}^-$  and  $V_{X(\theta)}^+$  as a function of the local oscillator phase  $\theta$ . The variances of the individual modes show no phase evolution and fluctuations greater than shot-noise. The two-mode variances are squeezed below shot-noise at  $\theta = 0.75\pi$  for  $V_{X(\theta)}^-$  and at  $\theta = 1.25\pi$  for  $V_{X(\theta)}^+$  (b) Inseparability parameter  $V_{X(\theta)}^- + V_{X(\theta+\pi/2)}^+$  as a function of the local oscillator phase  $\theta$ . The dashed line indicates inseparability of the underlying quantum state. We violate this boundary by 2.3 standard deviations which proves continuous-variable entanglement.

In this section, we prove the quantum nature of DCE by demonstrating the quantum correlations between the excitations created in the two modes. For these experiments, we employ the sequence of section 3.1, with a shorter modulation time of 110 ms. Following our previous work [17], we demonstrate the quantum correlations between the quadratures of the levels  $|1, \pm 1\rangle$ , defined as  $x_{\pm 1} = 1/\sqrt{2}(a_{\pm 1}^\dagger + a_{\pm 1})$  and  $p_{\pm 1} = i/\sqrt{2}(a_{\pm 1}^\dagger - a_{\pm 1})$ . In our experiments, we detect either the  $x$  or the  $p$  quadratures of both levels  $|1, \pm 1\rangle$  by unbalanced atomic homodyne detection. Our BEC acts as the local oscillator for the homodyne detection. A radio-frequency pulse couples 15% of the local oscillator with the levels  $|1, \pm 1\rangle$ . The local oscillator phase  $\theta$  can be adjusted via a variable holding time with deactivated microwave dressing. For each

holding time, we obtain a linear combination of both quadratures  $X_{\pm 1}(\theta) = x_{\pm 1} \cos(\theta - \pi/4) + p_{\pm 1} \sin(\theta - \pi/4)$ . For  $\theta = 3\pi/4$  ( $\theta = 5\pi/4$ ) the variance of the difference (sum) is squeezed. This local oscillator phase  $\theta$  can be associated with the  $x$  ( $p$ ) quadrature. The  $x$  and  $p$  quadratures show sub-shot-noise fluctuations (blue and purple dots in Fig. 4a), which indicates two-mode squeezing. Additionally, no phase dependence is visible for the quadrature correlations of the individual modes (red and orange dots in Fig. 4a). As a consequence, there is no one-mode squeezing, which follows our predictions. We prove entanglement with the inseparability criterion  $V_x^- + V_p^+ < 2$  [11, 12] for two collective atomic modes (see Fig. 4b). The strongest violation is  $V_x^- + V_p^+ = 1.51 \pm 0.17$  proving entanglement with 2.9 standard deviations.

#### 5. Conclusion

In conclusion, we have demonstrated that spin dynamics in spinor BECs resembles the DCE. We have observed the generation of atom pairs in initially empty excited states of the system by a resonant modulation of the energy of the excited states. The created pairs carry entanglement, which we have proven by detecting the non-classical correlations between the quadratures. This central finding unveils the deep connection between the Casimir Effect and the generation of non-classical states. In the future, the parametric generation of entangled atom pairs can be employed as a versatile tool for the generation of entangled atomic ensembles. The modulation method offers a fast initialization of the pair generation process compared to conventional methods, where the resonance conditions is reached by ramping the QZE to the unstable regime.

#### Acknowledgments

We also acknowledge support from the Centre for Quantum Engineering and Space-Time Research (QUEST), Generalitat de Catalunya through grant 2014SGR-401, the Ministerio de Economía (Spain) through grant FIS2014- 54672-P and the Deutsche Forschungsgemeinschaft (DFG) through project KL2421/2-1, RTG 1729, CRC 1227 (DQ-mat), project A02.

#### References

- [1] Casimir H B G and Polder D 1948 *Phys. Rev.* **73** 360–372
- [2] Lifshitz E M 1956 *Sov. Phys. JETP* **2** 73–83
- [3] Lamoreaux S K 1997 *Phys. Rev. Lett.* **78**(1) 5–8
- [4] Mohideen U and Roy A 1998 *Phys. Rev. Lett.* **81**(21) 4549–4552
- [5] Yablonovitch E 1989 *Phys. Rev. Lett.* **62**(15) 1742–1745

- [6] Schwinger J 1992 Proc. Natl. Acad. Sci. U.S.A. **89** 11118–11120
- [7] Wilson C M, Johansson G, Pourkabirian A, Simoen M, Johansson J R, Duty T, Nori F and Delsing P 2011 Nature **479** 376–379
- [8] Lähteenmäki P, Paraoanu G S, Hassel J and Hakonen P J 2013 Proc. Natl. Acad. Sci. U.S.A. **110** 4234–4238
- [9] Jaskula J C, Partridge G B, Bonneau M, Lopes R, Ruaudel J, Boiron D and Westbrook C I 2012 Phys. Rev. Lett. **109**(22) 220401
- [10] Hoang T M, Anquez M, Robbins B A, Yang X Y, Land B J, Hamley C D and Chapman M S 2016 Nat. Commun. **7** 11233
- [11] Simon R 2000 Phys. Rev. Lett. **84**(12) 2726–2729
- [12] Duan L M, Giedke G, Cirac J I and Zoller P 2000 Phys. Rev. Lett. **84**(12) 2722–2725
- [13] Hung C L, Gurarie V and Chin C 2013 Science **341** 1213–1215 0036-8075
- [14] Klempt C, Topic O, Gebreyesus G, Scherer M, Henninger T, Hyllus P, Ertmer W, Santos L and Arlt J J 2009 Phys. Rev. Lett. **103** 195302
- [15] Scherer M, Lücke B, Gebreyesus G, Topic O, Deuretzbacher F, Ertmer W, Santos L, Arlt J J and Klempt C 2010 Phys. Rev. Lett. **105** 135302
- [16] Scherer M, Lücke B, Peise J, Topic O, Gebreyesus G, Deuretzbacher F, Ertmer W, Santos L, Klempt C and Arlt J J 2013 Phys. Rev. A **88**(5) 053624
- [17] Peise J, Kruse I, Lange K, Lücke B, Pezzè L, Arlt J, Ertmer W, Hammerer K, Santos L, Smerzi A and Klempt C 2015 Nat. Commun. **6** 8984